analytical chemistry

Article

pubs.acs.org/ac

Ten-Atom Silver Cluster Signaling and Tempering DNA Hybridization

Jeffrey T. Petty,*,† Orlin O. Sergev, Andrew G. Kantor, Ian J. Rankine, Mainak Ganguly, Frederic D. David, Sandra K. Wheeler, and John F. Wheeler

Department of Chemistry, Furman University, Greenville, South Carolina 29613, United States

Supporting Information

ABSTRACT: Silver clusters with ∼10 atoms are molecules, and specific species develop within DNA strands. These molecular metals have sparsely organized electronic states with distinctive visible and near-infrared spectra that vary with cluster size, oxidation, and shape. These small molecules also act as DNA adducts and coordinate with their DNA hosts. We investigated these characteristics using a specific cluster-DNA conjugate with the goal of developing a sensitive and selective biosensor. The silver cluster has a single violet absorption band (λ_{max} = 400 nm), and its single-stranded DNA host has two domains that stabilize this cluster and hybridize with target oligonucleotides. These target analytes transform the weakly emissive violet cluster to a new chromophore with blue-green absorption (λ_{max} = 490 nm) and strong green emission (λ_{max} = 550 nm). Our studies consider the synthesis, cluster size, and DNA structure of the precursor violet cluster-DNA complex. This species preferentially forms with relatively low amounts of Ag^+, high concentrations of the oxidizing agent O_2, and DNA strands with ≳20 nucleotides. The resulting aqueous and gaseous forms of this chromophore have 10 silvers that coalesce into a single cluster. This molecule is not only a chromophore but also an adduct that coordinates multiple nucleobases. Large-scale DNA conformational changes are manifested in a 20% smaller hydrodynamic radius and disrupted nucleobase stacking. Multidentate coordination also stabilizes the single-stranded DNA and thereby inhibits hybridization with target complements. These observations suggest that the silver cluster-DNA conjugate acts like a molecular beacon but is distinguished because the cluster chromophore not only sensitively signals target analytes but also stringently discriminates against analogous competing analytes.

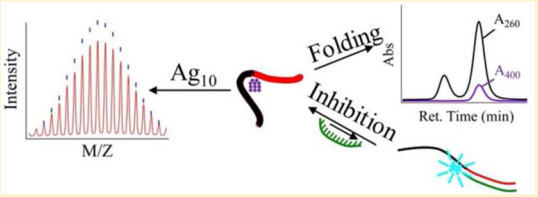

Biosensors identify chemical signatures that characterize food safety, air and water quality, and human diseases.[1,2] Their wide-ranging capabilities emanate from two fundamental functions, recognizing and identifying specific target analytes.[3,4] Our studies focus on recognition using DNA-based sensors and identification using silver cluster labels. Nucleic acids provide a synthetic platform to develop sensors for a broad range of analytes, and the targets are recognized through strong and specific biomolecular interactions.[5,6] For example, DNA hairpins bind oligonucleotide analytes via their single-stranded loops. They balance the stabilities of their intermolecular loop-analyte vs intramolecular stem duplexes and thereby discern oligonucleotides with single nucleotide differences.[7,8] Nucleic acid aptamers expand the scope of analytes because their distinctive tertiary structures define unique substrate binding sites.[9] Systematic evolution has yielded aptamers that discriminate species ranging from metal ions to cells and that distinguish closely related analytes such as theophylline and its methylated analogue caffeine.[10] Analytes not only associate with but can also structurally alter biosensors, and DNA conformational changes underlie highly sensitive detection strategies. For example, DNA hairpins hybridize with their complementary target and unfold from compact hairpins to open duplexes.[11−14] Such distinct conformations are tracked by exogenous labels such as organic dyes, semiconductor and noble metal nanoparticles, and conjugated polymers.[3,6] High-contrast signals develop through different mechanisms, such as when analytes alter the coupling between covalently bound labels or generate new chromophore binding sites.[6] We are particularly interested in optical signals because they offer high sensitivity over a large concentration range and the potential for remote, in vivo detection.[3,15] We consider the advantages of chromophore labels based on silver clusters.

Silver clusters with ∼10 atoms are molecules with discrete electronic states and their optical spectra vary with the number of silver atoms, net oxidation state, and cluster shape.[16−18] Such small clusters agglomerate without ligands, and DNA strands yield functional chromophores in two respects. First, oligonucleotides stabilize specific clusters. The electron-rich nucleobases coordinate silver atoms and restrain cluster growth, and the primary sequence and secondary structure of DNA strands define specific cluster binding sites.[19,20] A resulting suite of chromophores is spectrally diverse and optically bright. They absorb and emit throughout the visible to near-infrared region from 400−900 nm and have extinction coefficients of ∼10^5 M^{-1} cm^{-1}, fluorescence quantum yields of ∼40%, and fluorescence lifetimes of ∼1 ns.[19,21] Second, longer DNA strands both coordinate silver clusters and bind target analytes such as metal ions, peptides, and oligonucleotides.[5,22−27] Such analytes bind with the DNA strand and transform the cluster

Received: February 3, 2015
Accepted: April 29, 2015

DOI: 10.1021/acs.analchem.5b01265
Anal. Chem. XXXX, XXX, XXX−XXX

environment, as reflected in absorption red-shifts ≳100 nm and fluorescence magnifications ≳100-fold. These changes rival or exceed those from other chromophores and thus highlight a key advantage of silver cluster labels.[23,28−31] Our goal is to understand the basis for this optical transformation, and one underlying factor is DNA conformation. Remotely positioned mismatched base pairs, proximally positioned strands in duplexes, and the assembly of multiple strands show that distant, allosteric changes in DNA structure alter the chemical and electronic environments of cluster adducts.[20,22,32−35] Spectroscopic and thermodynamic studies bolster this link between the coordination and spectrum of the cluster adduct. Static quenching suggests that the analytes bind to the DNA host and drive the cluster to a new binding site.[22,23,36,37] Temperature reversibly switches the absorption spectra of precursor and product clusters, and van't Hoff analysis shows that the clusters change binding sites.[38] Elemental analysis of chromatographically purified conjugates shows that the cluster retains its stoichiometry through these optical changes.

This paper focuses on a specific silver cluster-DNA that not only optically signals but also inhibits association with target DNA strands. The DNA host is single-stranded and integrates a cytosine-rich cluster domain for its silver cluster adducts and a recognition site for complementary oligonucleotides.[19,21,23,39−41] The silver cluster is the optical reporter, and our studies evaluate a species with a single violet absorption band (λ_{max} = 400 nm). This violet cluster-DNA conjugate is a sensitive biosensor because target complementary strands hybridize with the single-stranded oligonucleotide and transform the weakly emissive violet chromophore to a new species with blue-green absorption (λ_{max} = 490 nm) and strong green emission (λ_{max} = 550 nm).[38] This cluster exhibits another molecular characteristic because it is a small adduct that develops within a larger DNA host. It folds and stabilizes the single-stranded DNA and inhibits association with target analytes. Thus, this violet cluster-DNA conjugate is also a discriminate biosensor because it shuns analogous competing analytes. We investigated this specific species with the goal of developing a spectrally diverse suite of sensitive and selective sensors.[19,21,31,42] We considered three issues to better understand optical switching and analyte discrimination by DNA-bound silver clusters. First, we conveniently and efficiently synthesized the precursor violet cluster-DNA complex by using low Ag^+/DNA concentrations with oxidizing agents. These studies have practical importance because chemical yield dictates the strength of the optical signal from the sensor. Furthermore, the cluster-DNA purity enabled our silver stoichiometry and DNA structural studies. Second, we measured the silver/DNA stoichiometry using absorption spectroscopy, isothermal titration calorimetry, atomic emission, and mass spectrometry. These measurements connect the empirical stoichiometry with the cluster size, an important benchmark for understanding the electronic structure and spectra of silver clusters. Additionally, these studies establish the formation of a DNA-based sensor in which an oligonucleotide encapsulates a silver cluster with a specific stoichiometry. Thus, this sensor is distinct from larger nanoparticles derivatized with DNA strands.[43] Third, we measured changes in DNA shape, structure, and reactivity using size exclusion chromatography, dynamic light scattering, circular dichroism, and absorption spectroscopy. These measurements suggest that the violet cluster sequesters the recognition site and thereby impedes hybridization with the target. These studies of synthesis, cluster size, and DNA structure provide insight that will promote the development of this distinctive class of biosensors.

EXPERIMENTAL SECTION

Materials. Lyophilized and desalted oligonucleotides (Integrated DNA Technologies) were hydrated, and concentrations were measured by the absorbances at 260 nm. Extinction coefficients were derived from the nearest-neighbor approximation.[44] A borate/boric acid buffer with pH = 9.8 disrupted aggregates favored by cytosine-rich strands.[45,46] The 20-nucleotide DNA strand used for the majority of these studies was CCCCAACTCCTTCCCGCCAC, where the strand polarity is 5′ → 3′. We also used variants of this oligonucleotide, and their sequences are provided in the figure captions. The clusters were prepared using $AgNO_3$ (Acros), and the reducing agent was $NaBH_4$ (Aldrich). These reagents were used as received.

Synthesis. Violet cluster conjugates were formed by combining 8 equiv of Ag^+ with 30 μM oligonucleotide in water. In this paper, the relative amounts of silver refer to the molar ratio of Ag^+/oligonucleotide. This solution was heated at 80 °C for 5 min to disrupt DNA aggregates and then cooled prior to BH_4^- reduction. Prior studies indicate that the relative amount of BH_4^- has a minor impact on the synthetic outcome.[41] The violet cluster was favored by exposing the solution to 500 psi O_2 at room temperature for 3 h. For mass spectrometry studies, these solutions were dialyzed to achieve 10^2−10^6 dilution of lower molecular weight species. The dialysis was accomplished using the Vivaspin 20 (Sartorius) at 25 °C and 4000 rpm. For the thermodynamic studies, violet cluster-DNA conjugates were diluted to 10 μM in a buffer with 10 mM citric acid/citrate at pH = 6.5 and 200 mM $NaClO_4$. The Na^+ promoted target hybridization with the recognition site. The resulting sample was heated to 50 °C for 20 min and then cooled to room temperature.

Characterization. Absorption spectra were acquired with a Cary 50 (Varian) at a scan rate of 600 nm/min using an appropriate buffer baseline and using plastic cuvettes (BrandTech). Circular dichroism spectra were acquired with a DSM 17 CD spectrophotometer (Olis). The spectra were collected from 600 to 220 nm using quartz cells with a path length of 1 cm using a scanning rate was ∼150 nm/min. A background spectrum of water was collected and subtracted from three averaged scans of the sample. Size exclusion chromatograms were collected with a Prominence high-performance liquid chromatography system (Shimadzu) using a 300 mm × 7.8 mm BioSep-SEC-S2000 column (Phenomenex), having 5 μm particles and a pore size of 145 Å. The mobile phase was buffered at pH = 6.5 with 10 mM citrate/citric acid that was supplemented with 300 mM $NaClO_4$ to minimize solute interactions with the stationary phase.[47,48] To assess hydrodynamic radii, size standards were based on thymine oligonucleotides dT_{10}, dT_{15}, dT_{20}, and dT_{30}.[20,49] For sample isolation, timing between the absorption spectrometer (SPD-M20A) and the fraction collection (FRC-10A) was determined using a concentrated solution of dye. To eliminate the preceding unlabeled DNA to form the desired cluster-labeled DNA, Gaussian fitting was used to temporally resolve the species and identify the optimal collection window. Following collection, the samples were analyzed using an inductively coupled plasma−optical emission spectrometer (Optima 7300 DV, PerkinElmer). Nitric acid was added to a

DOI: 10.1021/acs.analchem.5b01265
Anal. Chem. XXXX, XXX, XXX−XXX

final concentration of 10% (v/v), and a yttrium reference with emission at 371.03 nm was added to account for variations in the sample delivery rate. Silver and phosphorus standards (High Purity Standards) were used to generate calibration curves, and control samples containing oligonucleotide and Ag^+ were used to account for matrix effects.[50] A peristaltic pump delivered the samples to the nebulizer and the argon plasma. To relate the phosphorus and oligonucleotide concentrations, the lengths were derived from the DNA sequences, after accounting for the absence of the 3′ terminal phosphate. Silver and phosphorus were detected using their emissions at 328.07 and 213.62 nm, respectively, and the optical chamber was purged with nitrogen to detect the UV emission from phosphorus. These elements were detected with sensitivities of ∼30 nM P (20 ppb) and ∼10 nM Ag (1 ppb). Three samples were pooled for analysis. Phosphorus was exclusively associated with the phosphodiester backbone in DNA and thus served as a surrogate for the DNA concentration measurements. A total of 18 measurements were evaluated for the final silver/DNA stoichiometry, and a sample calculation is provided in Appendix B of the Supporting Information. Mass spectra were collected using Q-TOF G2-S (Waters) and analyzed with MassLynx V4.1. Samples were diluted with water to 0.3 μM oligonucleotide concentration and were infused via a syringe pump operated at 20 μL/min. The spectra were acquired in the negative ion mode with a capillary voltage of −2.7 kV, sampling cone voltage of −15 V, extraction cone voltage of 10 V, a cone gas flow of 45 L/h of cone gas, and a desolvation gas flow of 450 L/h. The source temperature was 80 °C and the desolvation temperature was 130 °C. Mass calibration was performed using aggregates of sodium formate in the 400 < m/z < 2000 range. Each mass spectrum was an average of 290 scans collected in V mode, and these spectra were processed with the MassLynx software. Calorimetry studies were conducted using a Microcal VP-ITC (Northhampton, MA) controlled by Origin 7.0 software.[51] Heat changes associated with the titration were determined by integrating the power required to maintain reference and sample cells at the same temperature. Heat changes associated with dilution of $AgNO_3$ were subtracted after saturation of the binding sites. A single-site binding model determined the enthalpy and free energy changes and the adduct stoichiometry. Dynamic light scattering studies were conducted with a Malvern Zetasizer Nano-ZS operating at 632.8 nm. The measurements were conducted at 25 °C in water. The hydrodynamic radius was derived from the diffusion coefficient based on the volume distribution and the Stokes−Einstein equation.[52]

RESULTS

A silver cluster with violet absorption complexed with the 20-nucleotide strand **CCCCAACTCCTT**-*CCCGCCAC*, where the 5′ bolded sequence is the cytosine-rich cluster domain and the 3′ italicized sequence is the target recognition site. This complex is a sensor for target DNA strands that hybridize with the recognition site (Figure 1). This paper focuses on the synthesis, silver stoichiometry, and DNA structure of this oligonucleotide-violet cluster complex.

Selective Violet Cluster Formation. Silvers coalesce and form clusters when DNA-bound Ag^+ is chemically reduced with BH_4.[19,21,39,53] This synthetic strategy typically yields multiple species with distinct spectra and structures, as illustrated by the above 20-nucleotide strand that produced violet (λ_{max} = 400 nm) and green (λ_{max} = 515 nm) absorptions.[19−21,53−55] We

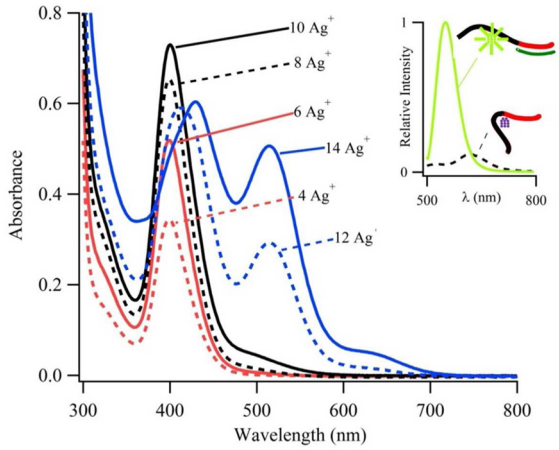

Figure 1. Absorption spectra of 30 μM solutions of the 20 nucleotide DNA with varying relative amounts of Ag^+. Concentrations $\lesssim$10 Ag^+/DNA favor the violet species with λ_{max} = 400 nm over its green counterpart with λ_{max} = 515 nm. The inset demonstrates that complementary strands (green) hybridize with the recognition site (red) and transform the weakly emissive violet cluster (black dotted spectrum) to a new species with strong green emission (solid green spectrum).

considered how four factors influenced the violet species (Figure 1). First, concentrations from 4 to 10 Ag^+/oligonucleotide predominantly yielded violet absorption with progressively increasing absorbances at λ_{max} = 400 nm. Concentrations >10 Ag^+/oligonucleotide promoted the green in lieu of the violet absorption. The concentration dependence of these spectra suggests that a smaller violet cluster developed at the lower Ag^+ concentrations while a larger green cluster formed at higher Ag^+ concentrations. Second, oxygen preserved the violet but diminished the green band (Figure S1 in the Supporting Information). A similar response with H_2O_2 suggests that these two reagents act as oxidizing agents and selectively destroyed the green but not the more robust violet cluster.[41] Third, the 20-nucleotide template established a preferred cluster environment (Figure S2 in the Supporting Information). Two abridged derivatives with 15 nucleotides shifted the absorption and diminished the absorbance, whereas two elongated derivatives with 24 and 28 nucleotides recovered the spectrum of the violet cluster. These spectra suggest that the 20 nucleotides harbored an optimal binding site for the violet cluster. Shorter strands truncated this site, while longer strands contained extraneous nucleobases. Fourth, solutions with pH = 3−8 do not alter the violet absorption (Figure S3 in the Supporting Information). This stability suggests that the DNA maintains its conformation and holds the favored binding site for the violet cluster.[20]

On the basis of these experiments, we preferentially formed the violet cluster by using the 20 nucleotide DNA with 8 Ag^+/DNA and 33 atm O_2. These reaction conditions yielded only the violet cluster but did not saturate the available DNA binding sites. Two DNA species were distinguished by size exclusion chromatography (Figure 2). The leading species at 9.0 min eluted at the same time as the native oligonucleotide and absorbed only in the UV region with λ_{max} = 260 nm, so it was ascribed to unlabeled DNA with no silver cluster adduct. The lagging species at 9.4 min absorbed both at λ_{max} = 260 nm and at 400 nm. This latter absorption band arose from the cluster adduct, so this species was ascribed to the DNA-violet

DOI: 10.1021/acs.analchem.5b01265
Anal. Chem. XXXX, XXX, XXX−XXX

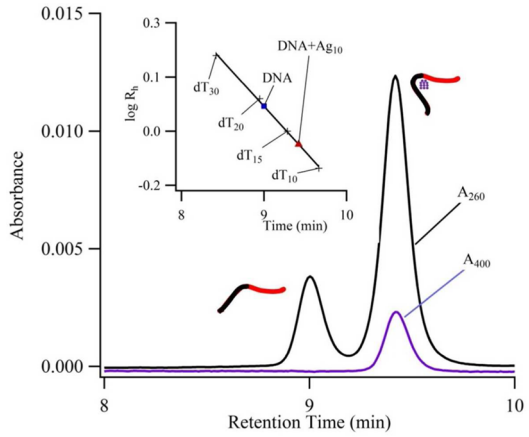

Figure 2. Size exclusion chromatograms distinguish the unligated (9.0 min) and ligated (9.4 min) DNA strands that result when 8 Ag^+ and 4 BH_4^- react with the 20-nucleotide DNA strand. The inset shows the calibration curve generated with the thymine oligonucleotides. The blue square represents the native DNA strand, and the red triangle represents the violet cluster-DNA conjugate.

cluster conjugate. This selective and efficient synthesis of this specific silver cluster anchored our silver stoichiometry and secondary DNA structural studies.

Cluster Stoichiometry. Absorption spectroscopy with isothermal titration calorimetry, elemental analysis, and mass spectrometry experiments measured the silver stoichiometry for both aqueous and gaseous complexes. The aqueous species was indirectly interrogated by measuring the violet absorption spectrum with varying Ag^+/DNA ratios (Figure 1). These concentrations governed the amount of bound Ag^+ and thus the number of reduced silvers. The association of Ag^+ with the 20-nucleotide DNA strand was measured by isothermal titration calorimetry. These measurements yielded a stoichiometry of 9.2 (±0.2) Ag^+/DNA and an affinity constant of 5.6 (±0.6) × 10^6 M^{-1}, which are consistent with earlier spectroscopic studies (Figure S4 in the Supporting Information).[56,57] With our conditions of 30 μM DNA and 240 μM Ag^+ (8 Ag^+/DNA), ~99% of the initial Ag^+ complexes with the oligonucleotide, so these bound Ag^+ had a local concentration of ~3 M within the ~1 nm hydrodynamic radius of the DNA host. We propose that this high concentration strongly favored quantitative conversion of the DNA-bound Ag^+ to reduced silver within the DNA strand. The DNA had a finite capacity for Ag^+, and the spectral transition from the violet to the green cluster suggests that 10 Ag^+ saturated the DNA binding site for the violet cluster. The high Ag^+-DNA affinity suggests that the violet cluster correspondingly had 10 silvers.

The silver stoichiometry of the aqueous species was also directly measured using elemental analysis. Our reaction conditions yielded a mixture of DNA strands with and without the violet cluster, and these were separated by size exclusion chromatography (Figure 2). The isolated cluster-DNA conjugate was analyzed by inductively coupled plasma-atomic emission spectroscopy. Phosphorus was the elemental surrogate for DNA, so emission intensities at 213.67 and 328.07 nm provided the concentrations for phosphorus/DNA and silver, respectively. These relative amounts yielded an empirical stoichiometry of 10 ± 1 Ag/DNA, which matched the results from the Ag^+-dependent spectra (see Appendix B of the Supporting Information). Collectively, these two results suggest that the aqueous violet cluster-DNA conjugate has 10 silvers.

The silver stoichiometry of the gaseous silver-DNA conjugate was precisely quantified by mass spectrometry (Figure 3). This

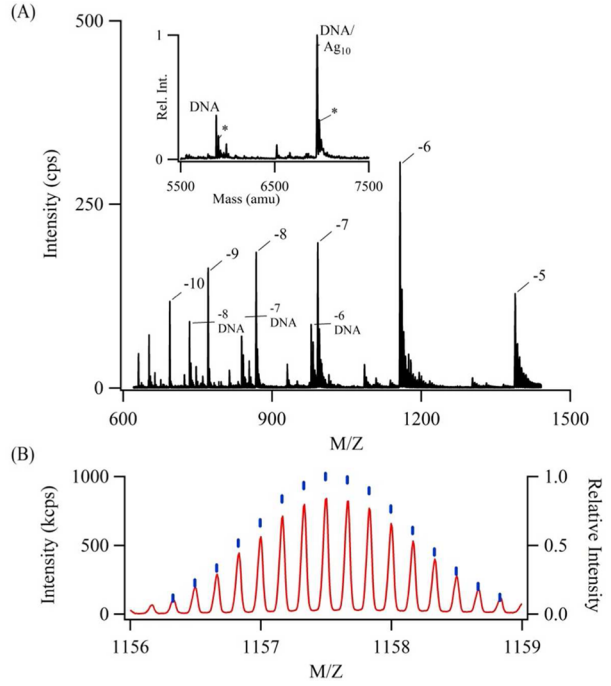

Figure 3. (A) Mass/charge spectrum of a violet cluster-DNA sample. The inset shows the composite spectrum of the unligated DNA at 5879 amu and the DNA with 10 Ag at 6951 amu. The * peaks represent Na^+ adducts. (B) Expanded view of the 6− charge state. The blue tick marks represent the predicted masses based on the molecular formula of the oligonucleotide with 10 silvers and 6 fewer hydrogens. The precision is 0.3 ± 0.4 ppm for the observed and predicted masses of the isotopologues.

species was produced by electrospray ionization from the aqueous solution, and the complex integrity was gauged by two observations. First, the DNA conjugate was stable over a range of instrumental settings, and we used gentle conditions that disfavored cluster fragmentation.[58] Second, ion intensities from the cluster-DNA complex correlated with violet absorbances (Figure S5 in the Supporting Information). These two observations suggested that the violet cluster survived the transition intact from the aqueous to gaseous states. The resulting mass spectrum exhibited a series of peaks from m/z = 600−1500. An analogous peak pattern for the native oligonucleotide suggested that varying numbers of H^+ protonated the phosphate backbones of both species.[59] Two aspects of this spectrum established the cluster stoichiometry. First, the charge state peaks were converged to the zero charge state, and the resulting spectrum identified the native DNA strand with a mass of 5879 amu and its 10-silver adduct with a mass of 6951 amu (Figure 3A). Like the mass spectrum, the chromatogram showed that the aqueous sample also has unlabeled and labeled DNA strands in a relative ratio of ~0.3, which is similar to the relative ion abundances of ~0.4. Thus, we suggest that the distribution of gaseous species was imprinted from the aqueous sample (Figures 2 and 3A). The conjugate mass was 6 amu lower than the combined mass of the native DNA strand and 10 silvers. Prior studies of other silver cluster-DNA conjugates attribute this difference to the loss of 6 H^+ from the phosphate backbone because the cluster

DOI: 10.1021/acs.analchem.5b01265
Anal. Chem. XXXX, XXX, XXX−XXX

was oxidized.[60,61] Second, the separate charge state peaks exhibited fine structure that depended on the natural abundances of 51.8% ^{107}Ag and 48.2% ^{109}Ag. The peak spacings and distributions followed a model based on the molecular formula of the oligonucleotide ($C_{187}H_{244}O_{118}N_{65}P_{19}$) with 10 Ag (Figure 3B and Figure S6 in the Supporting Information). The number of hydrogens was adjusted to account for the charges of the ionized phosphate backbone and the oxidized cluster adduct. The mass precision across these six charge states in Figure 3 was 0.3−2.7 ppm, which lies within the tolerance limits for the instrument. We also studied the violet cluster complex with a longer 28-nucleotide strand. Correspondingly, this host produced a cluster with the same absorption spectrum and with 10 silvers (Figures S2 and S7 in the Supporting Information). Consistent silver stoichiometries with different lengths of DNA templates suggest that 10 silvers coalesced into a single cluster and occupied a common binding site within the two oligonucleotides.[31]

DNA Folding. The violet cluster with 10 silvers is ∼5.4-fold lighter than its DNA host, and this mass difference suggests that a large DNA encapsulated the smaller cluster. We considered how this molecular adduct altered the shape, structure, and reactivity of the single-stranded oligonucleotide. Size exclusion chromatography revealed changes in DNA shape and hydrodynamic radii (Figure 2).[62] The violet cluster-DNA conjugate eluted ∼0.4 min later and was thus more compact than the unligated, native strand. This temporal shift was related to a size change using the single-stranded thymine oligonucleotides dT_{10}, dT_{15}, dT_{20}, and dT_{30}. These oligonucleotides were chromatographic size standards because they behaved as random coils with progressively increasing hydrodynamic radii.[49] These references predicted that the unlabeled, 20-nucleotide strand had a hydrodynamic radius of 1.2 nm and was analogous to dT_{20} (blue square, inset for Figure 2). Thus, the native 20-nucleotide DNA has no inherent structure and behaved as a random coil polymer. The thymine references also predicted that the cluster-laden strand had a hydrodynamic radius of 1.0 nm and thus was 20% smaller than the native DNA strand. Considering the uncertainty associated with small nanoparticles, dynamic light scattering measured a comparable hydrodynamic radius of 0.8 ± 0.4 nm. Thus, these two measurements suggested that the violet cluster coordinated and contracted its monomeric, single-stranded DNA host.

Circular dichroism spectra show that the cluster also altered the DNA structure (Figure 4). Circular dichroism in the ultraviolet region (∼260 nm) discriminates structural forms of DNA through differences in nucleobase stacking and dipole coupling, and these spectra distinguished the DNA structures of the unligated and cluster-ligated DNA strands.[63,64] The nucleobases in silver cluster-DNA conjugates dominate ultraviolet absorption, so we did not expect significant spectral overlap and interference due to the violet cluster chromophore.[31,50,65] The spectrum of the native, unlabeled 20-nucleotide strand exhibited a strong peak with positive ellipticity at 280 nm and a weaker peak with negative ellipticity at 250 nm. This spectrum was characteristic of single-stranded DNA and further substantiated the random-coil conformation that was deduced from chromatography studies (Figure 2).[66] The spectrum of the neat cluster-DNA sample exhibited a ∼3-fold lower ellipticity at 280 nm and lacked the peak at 250 nm. These changes may have emanated from two effects.[63] First, silver clusters preferentially coordinate nucleobases, so these adducts may have disrupted nucleobase stacking and dipole coupling. Second, the metallic cluster may have altered charge distributions and dipole moments of the nucleobases. In either scenario, large spectral changes from the unlabeled to labeled DNA strands suggested that the violet cluster coordinated and reorganized multiple nucleobases within its encapsulating DNA host. Such multidentate, long-range interactions may underlie the DNA folding (Figure 2). The circular dichroism spectrum exhibited an additional peak with negative ellipticity that coincided with the violet absorption band (Figures 1 and 4). We are now investigating this transition.[67]

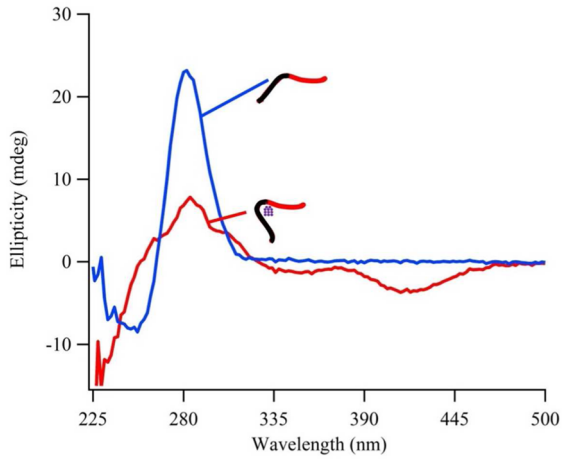

Figure 4. Circular dichroism spectra of the 20-nucletotide DNA strand without (blue) and with (red) the violet cluster adduct.

Thermodynamic studies with different recognition sites revealed another manifestation of folding. These studies exploited the modular sensor design in which the oligonucleotide has a 5′ cluster domain that prescribed a specific cluster environment and a 3′ recognition site that hybridized with the target complement (black and red sequences in Figure 5, respectively). Earlier thermodynamics studies showed that the violet cluster restrained hybridization, so we were interested in hybridization with the shorter recognition site within the 20-

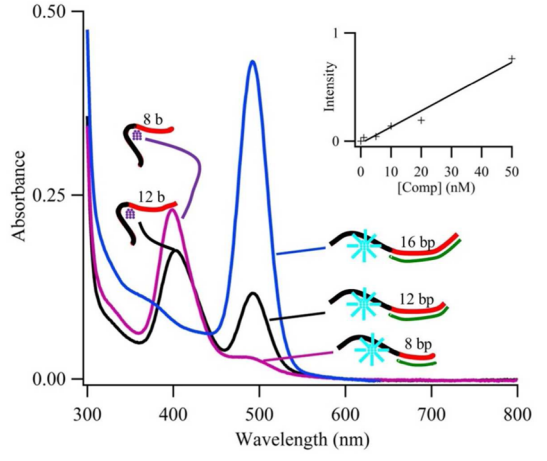

Figure 5. Absorption spectra with the single-stranded DNA hosts with 8 (violet), 12 (black), and 16 (blue) base pair recognition sites. Violet clusters within these single-stranded oligonucleotides converted to emissive blue-green clusters within the hybridized hosts, and the conversion efficiency increased with the complement length. The inset shows the sensitivity range using fluorescence (λ_{ex} = 490 nm and λ_{em} = 550 nm) for the 16 nucleotide recognition site.

DOI: 10.1021/acs.analchem.5b01265
Anal. Chem. XXXX, XXX, XXX−XXX

nucleotide strand. We compared its 8 nucleotide with 12 and 16 nucleotide recognition sites. All three sensor strands retained the 5′ cluster domain **CCCC AACT CCTT** and also harbored a common cluster binding site for the violet cluster (Figure S2 in the Supporting Information). These precursors also formed the same blue-green cluster when their complements hybridized the respective recognition sites. However, reaction efficiencies varied (Figure 5). Longer recognition sites and their complements more effectively converted the violet cluster to its blue-green counterpart with a fluorescence sensitivity of ∼10 nM for the target strand. We suggest that shorter oligonucleotides were less capable of converting the violet cluster because they have fewer base pairing and stacking interactions and lower duplex affinities. This link between duplex affinity and cluster transformation was substantiated with a mismatched complement (Figure S8 in the Supporting Information). Relative to the perfectly matched complement, the 16 nucleotide strand with two mismatches hybridized with an ∼7.7 kcal/mol less favorable affinity. We suggest that this lower affinity correspondingly inhibited the cluster transformation. Collectively, these complement length and mismatch measurements suggest that the cluster adduct restrained analyte recognition.[38]

DISCUSSION

A violet-absorbing silver cluster develops with DNA strands and becomes a functional chromophore in two respects. First, the cluster optically signals a target analyte that hybridizes with the DNA host. Second, the cluster stabilizes its single-stranded DNA host and discriminately recognizes specific target analytes. Our goal is to understand this optical switching and target discrimination, so we focused on the synthesis, silver stoichiometry, and DNA structure of a specific violet cluster-DNA conjugate.

This species was produced by combining Ag^+ with the single-stranded DNA followed by reduction with BH_4^-. This convenience is mollified by the formation of two clusters with violet and green absorptions, but we identified three factors that promote the violet cluster-DNA conjugate (Figures 1 and 2). First, concentrations covering the range from 4−10 Ag^+/DNA yield only the violet cluster. Specific clusters with 4 to 10 atoms have distinct spectra, so the exclusive formation of only the violet species in this concentration range highlights its inherent stability.[19,21,61] Second, DNA strands with ≳20 nucleotides form the violet cluster with similar efficiencies. This critical length suggests that the 20-nucleotide strand harbors a favored coordination environment for the violet cluster. Nucleobases coordinate and stabilize silver clusters, and DNA sequence and structure arrange these ligands into distinctive binding sites.[19,21,61] We are working under the constraints suggested by the ∼20 nucleotide length and exploring sequences that retain and possibly promote the stability of the violet cluster. Third, oxygen and hydrogen peroxide chemically target the green but retain the violet species. Both oxidizing agents may discriminate the violet and green clusters based on their sizes. Size and reactivity are linked for other silver and gold clusters because selective oxidation and etching can be used to produce high yields of specific clusters.[68−71] Collectively, these reaction conditions suggest that the molecular violet cluster encapsulated by the 20-nucleotide strand is inherently stable with respect to other clusters as well as oxidizing agents.

Our goal is to understand how the violet cluster optically switches to the blue-green cluster, and a key factor is the cluster size because it governs the electronic structure of silver clusters. We used three experiments to establish the silver stoichiometry. Ag^+-dependent absorption spectra and elemental analysis directly correlated the spectrum of the cluster in its aqueous environment with its stoichiometry. Mass spectrometry measurements utilized the high and specific yield of the violet cluster-DNA complex and provided precise masses and stoichiometries of the gaseous complex and its isotopologues. These three measurements with different DNA templates establish that the violet cluster is a single molecule with 10 silvers. We now consider this stoichiometry in light of cluster oxidation state that was deduced from the mass spectra. The overall mass and the isotope distribution showed that the ligated DNA has 10 silvers but 6 fewer hydrogens than its unligated counterpart. Hydrogens carry a 1+ charge and neutralize the phosphate backbone, so the absence of 6 H^+ suggests a counter 6+ charge for the cluster. An oxidized cluster is consistent with the use of the oxidizing agents O_2 and H_2O_2 that favor the violet cluster (Figure S1 in the Supporting Information). The oxidation state is consistent with prior measurements of other cluster-DNA conjugates.[60,61,67,72] These earlier mass and optical spectra studies support a structural model in which an oxidized Ag^+-nucleobase shell anchors a reduced silver core. These studies further propose that DNA coordination imposes rod-like shapes that control the electronic structure of the reduced silver core.[69,70,73] We are interested in learning how the violet cluster-DNA conjugate fits this novel structural and electronic model.

This violet cluster is a reporter with a high-contrast optical signal because it transforms to an emissive blue-green cluster when the target complement hybridizes with the single-stranded DNA (Figures 1 and 5). Violet clusters are also progenitors for other emissive DNA-bound silver clusters. For example, clusters with 11 ± 1 silvers and absorption at 400 nm develop with other DNA strands, but these are transformed to clusters with strong near-infrared absorption and emission.[31,38,42] Other emissively silent violet clusters transform into a suite of clusters with strong emission that spans the green to red spectral regions.[42] The diverse spectra of these successor clusters are simply dictated by the sequence of the 5′ cluster domains in the single-stranded sensor (black sequence in Figure 1). Collectively, these studies support the inherent stability of violet clusters with a range of single-stranded DNA hosts. However, this chromophore readily adapts to new DNA environments and morphs into starkly different chromophores with red-shifted absorption and strong emission. These apparently conflicting characteristics of stability and plasticity may be important for understanding and harnessing the potential of these biosensors.

The violet cluster is not only an optical label but is also an adduct that perturbs its DNA host. DNA structural changes were deduced from the circular dichroism spectra in the ultraviolet region and size exclusion chromatograms with DNA size standards. These experiments showed that the violet cluster disrupts nucleobase stacking and reduces the hydrodynamic radius of its DNA host by 20%. Other silver clusters also fold their DNA hosts, as shown by electrophoresis, chromatography, and diffusion studies.[20,55] Two competing factors may control such structural changes. On one hand, silver cations and clusters coordinate multiple nucleobases. Ag^+ linearly coordinates two nucleobases and forms stable, noncanonical base

DOI: 10.1021/acs.analchem.5b01265
Anal. Chem. XXXX, XXX, XXX−XXX

pairs between DNA strands.[74,75] Analogously, reduced silver clusters with near-infrared absorption and emission cross-link two cytosine-rich strands and form intermolecular dimers in dilute solutions with 500 nM oligonucleotide concentrations.[31,76,77] On the other hand, DNA strands mold their silver cluster adducts. The nucleobases anchor silver clusters, and cytosine forms the strongest complexes.[39,40,78] These nucleobases arrange into specific cluster environments according to the primary sequence and secondary structure of the DNA host.[19−21] Ligand organization is also important for gold nanoclusters because steric factors control the cluster size and spectra.[79,80] We are now modifying binding sites for the violet cluster by varying the sequence for its 20-nucleotide host. These studies may address the balance between cluster vs DNA control of the violet cluster environment.

These structural studies provide context for our thermodynamic results. Target oligonucleotides hybridize with the oligonucleotide recognition site within the DNA scaffold and convert the weakly emissive violet cluster to a new species with blue-green absorption and enhanced green emission. However, the conversion efficiency diminishes with the length and degree of complementarity of the target strand. We suggest that the complements act as crowbars that open the folded violet cluster-DNA complexes. In this model, the molecular equivalent of leverage depends on the complement affinity. This model supports our earlier findings that showed hybridization is restrained when DNA-bound clusters fold and stabilize their single-stranded host.[38] We suggest that this exogenous inhibition is a noncanonical, metal-nucleotide interaction and offers an opportunity to more selectively identify target analytes. Molecular beacons are a canonical analogue. These sensors distinguish analytes by balancing the stabilities of their duplex stem and target-loop duplex. The silver cluster sensor is distinctive because the ligand not only modulates DNA hybridization but also exhibits a high contrast optical response. We are now working to measure this stabilizing effect of the violet cluster and to identify its binding site. We hope that these studies will allow for a better understanding of the chemical and optical advantages of these sensors.

CONCLUSION

Our studies evaluated the synthesis, silver stoichiometry, and DNA structure of a specific complex between a violet silver cluster and a 20-nucleotide DNA strand. This type of complex is a distinctive biosensor because it both reports target oligonucleotides through spectral shifts and fluorescence enhancements while also modulating target hybridization through DNA folding. We postulate that this cluster is a member of a larger suite of silver clusters with violet absorptions that transform to highly emissive counterparts. The spectra of these successors span the blue-green to near-infrared regions and can be simply tuned by changing the DNA sequence. Thus, silver cluster-DNA sensors offer the possibility of sensitivity, selectivity, and spectral diversity. Our studies highlight key issues that will advance the development of these new class of sensors.

ASSOCIATED CONTENT

Supporting Information

Two sections: Appendix A, 8 figures describe absorption spectra with and without oxidizing agents, absorption spectra with different DNA templates, absorption spectra with different buffers, an isothermal titration calorimetry binding isotherm, mass spectra of the 5−, 7−, 8−, 9−, and 10− charge states of the violet cluster-DNA complex, correlation of mass and optical spectra of the gas and solution phase species, mass spectrum of the 28-nucleotide DNA-violet cluster complex, and absorption spectra with complementary and mismatched strands; Appendix B, calibration curves and an example calculation for the ICP analysis. The Supporting Information is available free of charge on the ACS Publications website at DOI: 10.1021/acs.analchem.5b01265.

AUTHOR INFORMATION

Corresponding Author

*E-mail: jeff.petty@furman.edu. Phone: 864-294-2689.

Author Contributions

The manuscript was written through contributions of all authors. All authors have given approval to the final version of the manuscript.

Notes

The authors declare no competing financial interest.

[†]J.T.P.: Henry Keith and Ellen Hard Townes Professor of Chemistry.

ACKNOWLEDGMENTS

We thank the National Institutes of Health (Grant 1R15GM102818), the National Science Foundation (Grant CBET-0853692), and the Beckman Foundation for support of this work. In addition, we thank the National Science Foundation (Grants CHE-0718588 and CHE-0922834). O.O.S. and A.K. were supported by undergraduate research fellowships provided through a USE Award to Furman University from the Howard Hughes Medical Institute. J.T.P. is grateful for the support provided by the Henry Keith and Ellen Hard Townes Professorship.

REFERENCES

(1) Sassolas, A.; Leca-Bouvier, B. D.; Blum, L. J. *Chem. Rev.* **2008**, *108*, 109−139.
(2) MacKay, S.; Wishart, D.; Xing, J. Z.; Chen, J. *IEEE Trans. Biomed. Circ. Syst.* **2014**, *8*, 4−14.
(3) Borisov, S. M.; Wolfbeis, O. S. *Chem. Rev.* **2008**, *108*, 423−461.
(4) Lubin, A. A.; Plaxco, K. W. *Acc. Chem. Res.* **2010**, *43*, 496−505.
(5) Liu, J. *TrAC, Trends Anal. Chem.* **2014**, *58*, 99−111.
(6) Liu, J.; Cao, Z.; Lu, Y. *Chem. Rev.* **2009**, *109*, 1948−1998.
(7) Tsourkas, A. *Development and optimization of dual FRET-molecular beacons for the detection and visualization of single-stranded nucleic acid targets*. Ph.D. Thesis, Georgia Institute of Technology and Emory University, 2002.
(8) Tsourkas, A.; Behlke, M. A.; Bao, G. *Nucleic Acids Res.* **2002**, *30*, 4208−4215.
(9) Jenison, R.; Gill, S.; Pardi, A.; Polisky, B. *Science* **1994**, *263*, 1425−1429.
(10) Feng, C. J.; Dai, S.; Wang, L. *Biosens. Bioelectron.* **2014**, *59*, 64−74.
(11) Plaxco, K. W.; Soh, H. T. *Trends Biotechnol.* **2011**, *29*, 1−5.
(12) Oh, K. J.; Cash, K. J.; Plaxco, K. W. *Chem.−Eur. J.* **2009**, *15*, 2244−2251.
(13) Tyagi, S. *Nat. Methods* **2009**, *6*, 331−338.
(14) Wang, K.; Tang, Z.; Yang, C. J.; Kim, Y.; Fang, X.; Li, W.; Wu, Y.; Medley, C. D.; Cao, Z.; Li, J.; Colon, P.; Lin, H.; Tan, W. *Angew. Chem., Int. Ed.* **2009**, *48*, 856−870.
(15) Algar, W. R.; Tavares, A. J.; Krull, U. J. *Anal. Chim. Acta* **2010**, *673*, 1−25.
(16) Zheng, J.; Nicovich, P. R.; Dickson, R. M. *Annu. Rev. Phys. Chem.* **2007**, *58*, 409.

DOI: 10.1021/acs.analchem.5b01265
Anal. Chem. XXXX, XXX, XXX−XXX

(17) Ramazanov, R. R.; Kononov, A. I. *J. Phys. Chem. C* **2013**, *117*, 18681−18687.
(18) Bonacic-Koutecky, V.; Pittner, J.; Boiron, M.; Fantucci, P. *J. Chem. Phys.* **1999**, *110*, 3876−3886.
(19) Richards, C. I.; Choi, S.; Hsiang, J.-C.; Antoku, Y.; Vosch, T.; Bongiorno, A.; Tzeng, Y.-L.; Dickson, R. M. *J. Am. Chem. Soc.* **2008**, *130*, 5038−5039.
(20) Sengupta, B.; Springer, K.; Buckman, J. G.; Story, S. P.; Abe, O. H.; Hasan, Z. W.; Prudowsky, Z. D.; Rudisill, S. E.; Degtyareva, N. N.; Petty, J. T. *J. Phys. Chem. C* **2009**, *113*, 19518−19524.
(21) Sharma, J.; Yeh, H. C.; Yoo, H.; Werner, J. H.; Martinez, J. S. *Chem. Commun.* **2010**, *46*, 3280−3282.
(22) Sharma, J.; Yeh, H. C.; Yoo, H.; Werner, J. H.; Martinez, J. S. *Chem. Commun.* **2011**, *47*, 2294−2296.
(23) Yeh, H. C.; Sharma, J.; Han, J. J.; Martinez, J. S.; Werner, J. H. *Nano Lett.* **2010**, *10*, 3106−3110.
(24) Lan, G.-Y.; Chen, W.-Y.; Chang, H.-T. *Biosens. Bioelectron.* **2011**, *26*, 2431−2435.
(25) Park, J.; Lee, J.; Ban, C.; Kim, W. J. *Biosens. Bioelectron.* **2013**, *43*, 419−424.
(26) Zhang, L.; Zhu, J.; Guo, S.; Li, T.; Li, J.; Wang, E. *J. Am. Chem. Soc.* **2013**, *135*, 2403−2406.
(27) Chen, J.; Zhang, X.; Cai, S.; Wu, D.; Chen, M.; Wang, S.; Zhang, J. *Biosens. Bioelectron.* **2014**, *57*, 226−231.
(28) Obliosca, J. M.; Liu, C.; Batson, R. A.; Babin, M. C.; Werner, J. H.; Yeh, H.-C. *Biosensors* **2013**, *3*, 185−200.
(29) Petty, J. T.; Story, S. P.; Hsiang, J. C.; Dickson, R. M. *J. Phys. Chem. Lett.* **2013**, *4*, 1148−1155.
(30) Tyagi, S.; Kramer, F. R. *Nat. Biotechnol.* **1996**, *14*, 303−308.
(31) Petty, J. T.; Giri, B.; Miller, I. C.; Nicholson, D. A.; Sergev, O. O.; Banks, T. M.; Story, S. P. *Anal. Chem.* **2013**, *85*, 2183−2190.
(32) Guo, W.; Yuan, J.; Dong, Q.; Wang, E. *J. Am. Chem. Soc.* **2010**, *132*, 932−934.
(33) Hsin-Chih, Y.; Sharma, J.; Han, J. J.; Martinez, J. S.; Werner, J. H. *Nanotechnol. Mag., IEEE* **2011**, *5*, 28−33.
(34) Li, J.; Zhong, X.; Zhang, H.; Le, X. C.; Zhu, J.-J. *Anal. Chem.* **2012**, *84*, 5170−5174.
(35) Yeh, H.-C.; Sharma, J.; Shih, I.-M.; Vu, D. M.; Martinez, J. S.; Werner, J. H. *J. Am. Chem. Soc.* **2012**, *134*, 11550−11558.
(36) Guo, W.; Yuan, J.; Wang, E. *Chem. Commun.* **2009**, *23*, 3395−3397.
(37) Petty, J. T.; Sengupta, B.; Story, S. P.; Degtyareva, N. N. *Anal. Chem.* **2011**, *83*, 5957−5964.
(38) Petty, J. T.; Sergev, O. O.; Nicholson, D. A.; Goodwin, P. M.; Giri, B.; McMullan, D. R. *Anal. Chem.* **2013**, *85*, 9868−9876.
(39) Petty, J. T.; Zheng, J.; Hud, N. V.; Dickson, R. M. *J. Am. Chem. Soc.* **2004**, *126*, 5207−5212.
(40) Soto-Verdugo, V.; Metiu, H.; Gwinn, E. *J. Chem. Phys.* **2010**, *132*, 195102.
(41) Petty, J. T.; Story, S. P.; Juarez, S.; Votto, S. S.; Herbst, A. G.; Degtyareva, N. N.; Sengupta, B. *Anal. Chem.* **2012**, *84*, 356−364.
(42) Obliosca, J. M.; Babin, M. C.; Liu, C.; Liu, Y. L.; Chen, Y. A.; Batson, R. A.; Ganguly, M.; Petty, J. T.; Yeh, H. C. *ACS Nano* **2014**, *8*, 10150−10160.
(43) Howes, P. D.; Chandrawati, R.; Stevens, M. M. *Science* **2014**, 346.
(44) Bloomfield, V. A.; Crothers, D. M.; Tinoco, J. *Ignacio Nucleic Acids: Structures, Properties, and Functions*; University Science Books: Sausaltio, CA, 2000.
(45) Brown, D. M.; Gray, D. M.; Patrick, M. H.; Ratliff, R. L. *Biochemistry* **1985**, *24*, 1676−1683.
(46) Gueron, M.; Leroy, J. L. *Curr. Opin. Struct. Biol.* **2000**, *10*, 326−331.
(47) Leroy, J. L.; Gehring, K.; Kettani, A.; Gueron, M. *Biochemistry* **1993**, *32*, 6019−6031.
(48) Yamane, T.; Davidson, N. *Biochim. Biophys. Acta* **1962**, *55*, 609−621.
(49) Doose, S.; Barsch, H.; Sauer, M. *Biophys. J.* **2007**, *93*, 1224−1234.
(50) Petty, J. T.; Fan, C.; Story, S. P.; Sengupta, B.; St. John Iyer, A.; Prudowsky, Z.; Dickson, R. M. *J. Phys. Chem. Lett.* **2010**, *1*, 2524−2529.
(51) Loo, K.; Degtyareva, N.; Park, J.; Sengupta, B.; Reddish, M.; Rogers, C. C.; Bryant, A.; Petty, J. T. *J. Phys. Chem. B* **2010**, *114*, 4320−4326.
(52) Thunemann, A. F.; Rolf, S.; Knappe, P.; Weidner, S. *Anal. Chem.* **2009**, *81*, 296−301.
(53) Gwinn, E. G.; O'Neill, P.; Guerrero, A. J.; Bouwmeester, D.; Fygenson, D. K. *Adv. Mater.* **2008**, *20*, 279−283.
(54) Ritchie, C. M.; Johnsen, K. R.; Kiser, J. R.; Antoku, Y.; Dickson, R. M.; Petty, J. T. *J. Phys. Chem. C* **2007**, *111*, 175−181.
(55) Driehorst, T.; O'Neill, P.; Goodwin, P. M.; Pennathur, S.; Fygenson, D. K. *Langmuir* **2011**, *27*, 8923−8933.
(56) Daune, M.; Kekker, C. A.; Schachman, H. K. *Biopolymers* **1966**, *4*, 51−76.
(57) Torigoe, H.; Okamoto, I.; Dairaku, T.; Tanaka, Y.; Ono, A.; Kozasa, T. *Biochimie* **2012**, *94*, 2431−2440.
(58) Guo, J.; Kumar, S.; Bolan, M.; Desireddy, A.; Bigioni, T. P.; Griffith, W. P. *Anal. Chem.* **2012**, *84*, 5304−5308.
(59) Beck, J. L.; Colgrave, M. L.; Ralph, S. F.; Sheil, M. M. *Mass Spectrom. Rev.* **2001**, *20*, 61−87.
(60) Schultz, D.; Gardner, K.; Oemrawsingh, S. S. R.; Markešević, N.; Olsson, K.; Debord, M.; Bouwmeester, D.; Gwinn, E. *Adv. Mater.* **2013**, *25*, 2797−2803.
(61) Copp, S. M.; Schultz, D.; Swasey, S.; Pavlovich, J.; Debord, M.; Chiu, A.; Olsson, K.; Gwinn, E. *J. Phys. Chem. Lett.* **2014**, *5*, 959−963.
(62) Harris, D. K. *Quantitative Chemical Analysis*; W.H. Freeman & Company, 1998.
(63) Cantor, C. R.; Schimmel, P. R. *Biophysical Chemistry*; 1st ed.; W. H. Freeman and Company: New York, 1980.
(64) Bishop, G. R.; Chaires, J. B. Characterization of DNA Structures by Circular Dichroism. In *Current Protocols in Nucleic Acid Chemistry*; John Wiley & Sons, Inc.: Hoboken, NJ, 2003; Vol. *7*, 7.11.1−7.11.8.
(65) O'Neill, P. R.; Gwinn, E. G.; Fygenson, D. K. *J. Phys. Chem. C* **2011**, *115*, 24061−24066.
(66) Gray, D. M.; Ratliff, R. L.; Vaughan, M. R. Circular dichroism spectroscopy of DNA. In *Methods in Enzymology*; David, M. J., Lilley, J. E. D., Eds.; Academic Press: New York, 1992; Vol. *211*, pp 389−406.
(67) Swasey, S. M.; Karimova, N.; Aikens, C. M.; Schultz, D. E.; Simon, A. J.; Gwinn, E. G. *ACS Nano* **2014**, *8*, 6883−6892.
(68) Jin, R.; Qian, H.; Wu, Z.; Zhu, Y.; Zhu, M.; Mohanty, A.; Garg, N. *J. Phys. Chem. Lett.* **2010**, *1*, 2903−2910.
(69) Yang, H.; Wang, Y.; Huang, H.; Gell, L.; Lehtovaara, L.; Malola, S.; Häkkinen, H.; Zheng, N. *Nat. Commun.* **2013**, *4*, 2422.
(70) Desireddy, A.; Conn, B. E.; Guo, J.; Yoon, B.; Barnett, R. N.; Monahan, B. M.; Kirschbaum, K.; Griffith, W. P.; Whetten, R. L.; Landman, U.; Bigioni, T. P. *Nature* **2013**, *501*, 399−402.
(71) Henglein, A.; Mulvaney, P.; Linnert, T. *Faraday Discuss.* **1991**, 31−44.
(72) Walter, M.; Akola, J.; Lopez-Acevedo, O.; Jadzinsky, P. D.; Calero, G.; Ackerson, C. J.; Whetten, R. L.; Gronbeck, H.; Hakkinen, H. *Proc. Natl. Acad. Sci. U.S.A.* **2008**, *105*, 9157−9162.
(73) Jadzinsky, P. D.; Calero, G.; Ackerson, C. J.; Bushnell, D. A.; Kornberg, R. D. *Science* **2007**, *318*, 430−433.
(74) Lippert, B. *Coord. Chem. Rev.* **2000**, *200−202*, 487−516.
(75) Megger, D. A.; Fonseca Guerra, C.; Bickelhaupt, F. M.; Müller, J. *J. Inorg. Biochem.* **2011**, *105*, 1398−1404.
(76) Schultz, D.; Gwinn, E. G. *Chem. Commun.* **2012**, *48*, 5748−5750.
(77) Petty, J. T.; Nicholson, D. A.; Sergev, O. O.; Graham, S. K. *Anal. Chem.* **2014**, *86*, 9220−9228.
(78) Sengupta, B.; Ritchie, C. M.; Buckman, J. G.; Johnsen, K. R.; Goodwin, P. M.; Petty, J. T. *J. Phys. Chem. C* **2008**, *112*, 18776−18782.
(79) Crasto, D.; Dass, A. *J. Phys. Chem. C* **2013**, *117*, 22094−22097.
(80) Krommenhoek, P. J.; Wang, J.; Hentz, N.; Johnston-Peck, A. C.; Kozek, K. A.; Kalyuzhny, G.; Tracy, J. B. *ACS Nano* **2012**, *6*, 4903−4911.

DOI: 10.1021/acs.analchem.5b01265
Anal. Chem. XXXX, XXX, XXX−XXX